ORIGINAL RESEARCH

Impaired Biofilm Development on Graphene Oxide-Metal Nanoparticle Composites

Agata Lange [ID][1], Marta Kutwin[1], Katarzyna Zawadzka[1], Agnieszka Ostrowska [ID][1], Barbara Strojny-Cieślak [ID][1], Barbara Nasiłowska [ID][2], Aneta Bombalska[3], Sławomir Jaworski [ID][1]

[1]Department of Nanobiotechnology, Institute of Biology, Warsaw University of Life Sciences, Warsaw, Poland; [2]Center for Biomedical Engineering, Institute of Optoelectronics, Military University of Technology, Warsaw, Poland; [3]Department of Optoelectronic Technologies, Institute of Optoelectronics, Military University of Technology, Warsaw, Poland

Correspondence: Agata Lange, Department of Nanobiotechnology, Institute of Biology, Warsaw University of Life Sciences, Ciszewskiego 8, Warsaw, 02-786, Poland, Tel +48 22 593 66 69, Email agata_lange@sggw.edu.pl

Purpose: Biofilms are one of the main threats related to bacteria. Owing to their complex structure, in which bacteria are embedded in the extracellular matrix, they are extremely challenging to eradicate, especially since they can inhabit both biotic and abiotic surfaces. This study aimed to create an effective antibiofilm nanofilm based on graphene oxide-metal nanoparticles (GOM-NPs).

Methods: To create nanofilms, physicochemical analysis was performed, including zeta potential (Zp) (and the nanocomposites stability in time) and size distribution measurements, scanning transmission electron microscopy (STEM), energy dispersive X-ray analysis (EDX), and atomic force microscopy (AFM) of the nanofilm surfaces. During biological analysis, reactive oxygen species (ROS) and antioxidant capacity were measured in planktonic cells treated with the nanocomposites. Thereafter, biofilm formation was checked via crystal violet staining, biofilm thickness was assessed by confocal microscopy using double fluorescent staining, and biofilm structure was analyzed by scanning electron microscopy.

Results: The results showed that two of the three nanocomposites were effective in reducing biofilm formation (GOAg and GOZnO), although the nanofilms were characterized by the roughest surface, indicating that high surface roughness is unfavorable for biofilm formation by the tested bacterial species (*Staphylococcus aureus* (ATCC 25923), *Salmonella enterica* (ATCC 13076), *Pseudomonas aeruginosa* (ATCC 27853)).

Conclusion: The performed analysis indicated that graphene oxide may be a platform for metal nanoparticles that enhances their properties (eg colloidal stability, which is maintained over time). Nanocomposites based on graphene oxide with silver nanoparticles and other types of nanocomposites with zinc oxide were effective against biofilms, contributing to changes throughout the biofilm structure, causing a significant reduction in the thickness of the structure, and affecting cell distribution. A nanocomposite consisting of graphene oxide with copper nanoparticles inhibited the biofilm, but to a lesser extent.

Keywords: biofilm, graphene oxide, metal nanoparticles, nanocomposites, nanofilms

Introduction

Bacterial cells living in liquid medium have enabled us to discover basic life functions, including metabolic aspects and genetic features connected with microorganisms. However, in nature, bacteria mostly exist in the form of complicated multicellular communities known as biofilms.[1] Biofilm-forming bacteria are embedded in self-produced extracellular polymeric substances (EPSs), which constitute a matrix for a specific cellular community.[2] EPS consists mostly of water due to highly hydrated biopolymers, which consequently allows water to be retained in the matrix.[3] Because of the formation of a spatial structure consisting of many components (polysaccharides, lipids, proteins, and extracellular DNA), EPS has a protective function against adverse environmental factors while at the same time creating a distinct habitat for bacteria anchored in the biofilm. However, bacteria embedded in a biofilm structure exhibit different properties than planktonic forms, especially when considering the lower parts of the structure, where cells exhibit lower metabolic activity, which increases to enhance resistance to both unfavorable environmental conditions and

Graphical Abstract
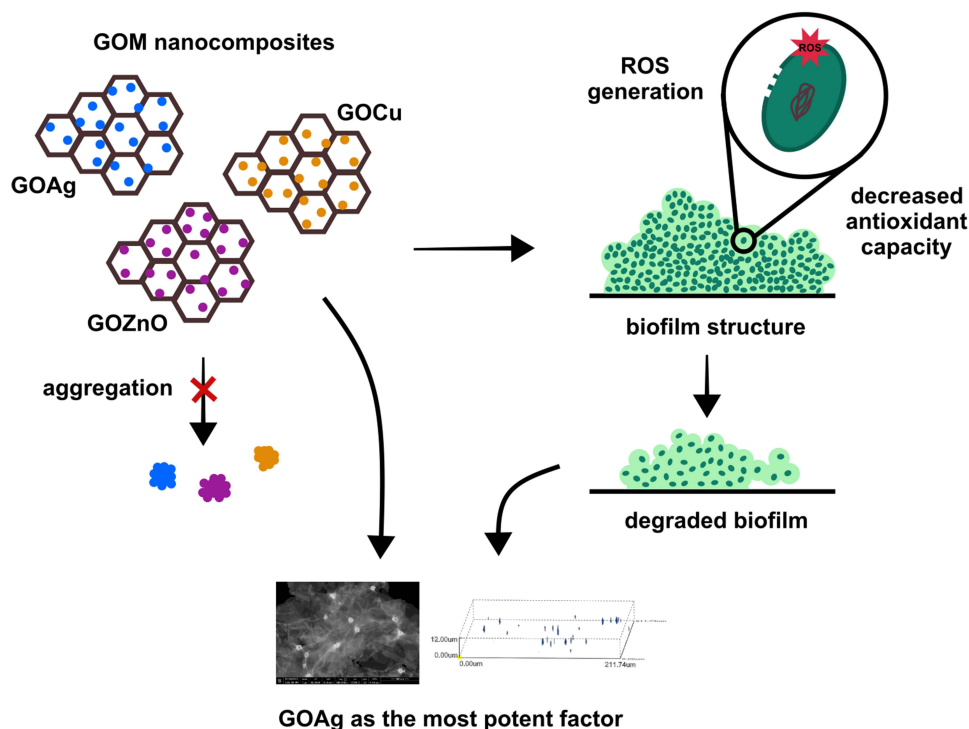
antibiotics.[4] The National Institutes of Health (NIH) announced that more than 80% of bacterial diseases are caused by biofilms. Most bacteria may create a biofilm structure on both biotic and abiotic surfaces, including medical or indwelling devices as well as the urinary and respiratory tracts and skin. In this state, bacterial cells are not even fought by the immune system's cells.[5] Bacteria that form biofilms on the surface of medical devices often belong to species such as *Staphylococcus aureus, Staphylococcus epidermidis, Escherichia coli*, or *Pseudomonas aeruginosa*.[6] As the vast majority of bacteria species can create biofilms, biofilms are also frequently multispecies. Biofilms produced by *S. aureus* are the etiological agent of many recurrent infections. These include infection of the bone knowns as osteomyelitis, but also periodontitis and peri-implantitis, chronic wound infection, chronic rhinosinusitis, endocarditis, ocular infection and indwelling medical device infection. The latter includes biofilm formed on orthopedic implants including prosthetic joints, wires, pins, external fixators, plates, screws, nails and mini-large fragment implants, on which biofilm formed by *S. aureus* is a major problem and cause of failure of the mentioned implants.[7] *P. aeruginosa* is a well-known biofilm former, which makes it an excellent candidate model to examine biofilm formation. The biofilm formed by *P. aeruginosa* is found in the polymicrobial environment of cystic fibrosis in the lungs. Similar to the previous bacterium mentioned, *P. aeruginosa* colonizes various medical surfaces, including (urinary catheters, implants, contact lenses, as well as food industry equipment (mixing tanks, vats and tubing).[8] Nontyphoidal biofilms produced by *Salmonella*, which is an enteric pathogen, pose a particular threat in the food processing and packaging industry. Such biofilms have been shown to adhere to abiotic materials used in the industry, including stainless steel, polystyrene or glass. Despite disinfection practices in the food industry, biofilms are much more resistant than planktonic forms, rendering commonly used practices ineffective.[9]

Therefore, biofilms are responsible for most diseases, especially chronic antibiotic-resistant infections, implying that they cannot be cured with conventional antibiotics. The difficulty of combating biofilms is not only based on the multidimensionality of their structure but also on the several stages of development that biofilms exhibit. Therefore, it is recommended that agents with antibiofilm properties have more than one impact point, which may include inhibition of

the quorum-sensing pathway, degradation of EPS, disruption of single bacterial cells, or decomposition and disorganization of biofilm structure.[10]

Bacteria in biofilms are 10–1000 times more resistant to antibiotics than are free-floating cells. Nevertheless, some strategies have been developed to help destroy biofilm structures and bacterial cells. These include, among others, photodynamic and photothermal therapies, antimicrobial peptides, nanoparticles (NPs) and plant extracts.[11,12] Due to the high reactivity of nanoparticles, they may interact with a biofilm's extracellular matrix (ECM), which contains multiple polymeric molecules with different charges. Most bacteria have a negatively charged ECM owing to the presence of chemical compounds, such as uronic acid and metal-bound pyruvate, which allows the creation of electrostatic forces with positively charged metal ions and organic compounds.[13] Antimicrobials may be transported within the biofilm structure. However, this was affected by the presence of sufficiently wide water channels that allowed the substance to reach the deeper layers. Unfortunately, due to the complex structure and continuous rearrangement of the structure, in the lower layers, there are often pores filled with water instead of the mentioned channels, resulting in dilution of the concentration of antimicrobial agents.[14] For this reason, not only an active strategy (which involves applying antimicrobial agents directly) is used but also a passive one, which involves the production of coatings disrupting the first step of biofilm formation, which is attachment and surface biofouling.[15] Coating implants and devices with agents exhibiting antibacterial/antibiofilm properties is a promising approach for infection prevention, and research is currently underway on strategies that could have an impact in this way.[6]

In general, nanoparticles' effect on biofilms may be two-folds: on the one hand, nanoparticles can prevent the formation of a biofilm structure before it emerges; on the other hand, they can destroy a well-formed biofilm structure.[16] Nanoparticles may be able to harm cells at several levels, indicating that they have non-specific effects. Metal nanoparticles may not only damage cell structures, such as walls and membranes, proteins, enzymes, DNA, and ribosomes, but also interfere with processes and pathways essential to the cell's proper functioning, as well as contribute to reactive oxygen species (ROS) production.[17] The main nanoparticles used as antibacterial agents are silver, gold, copper and zinc nanoparticles. Silver nanoparticles exhibit remarkable antibacterial properties, both against planktonic forms and the biofilm structure due to their penetration of the biofilm matrix. Gold nanoparticles are also characterized by their ability to destroy biofilm structure and impair bacterial metabolic activity, but their high price means they are usually not chosen as a first choice agent.[18] Copper nanoparticles, on the other hand, release toxic ions that bind to bacterial cell membranes and increase their permeability by entering the cell interior, where they bind to large molecules containing sulfhydryl and phosphate residues destroying protein and DNA structure. Copper nanoparticles can also be effective against multidrug-resistant microorganisms.[19] Zinc oxide nanoparticles show strong antibacterial activity against both Gram-negative and Gram-positive bacteria also due to ion release but also generation of reactive oxygen species. However, a common problem with metal oxide nanoparticles is their oxidation under sunlight.[18]

The physicochemical properties of NPs are particularly crucial because of their potential toxicity. Nanoparticle agglomeration influences their uptake and distribution, and consequently impacts their toxicity,[20] often changing their intended properties. However, the unique properties of nanoparticles can be maintained and even enhanced by the synergistic effect they can display when combined with materials, such as graphene or graphene oxide. The benefits of combining the two materials are significantly advantageous compared to the use of single materials, thereby significantly increasing their application potential.[21] Graphene materials have a flake structure with a large specific surface area, making them suitable structures for decoration with metal nanoparticles.[22] What is more, combining graphene materials with metal nanoparticles improves the functional properties of the components.[23] Despite the possibility of combining GO with other substances, GO itself can result in an antibacterial effect, in which several mechanisms are highlighted. One of them is mechanical damage to the structures of the outer layers of cells due to the sharp edges that GO has. In addition to this, in the planktonic form of bacteria, the predominant antibacterial effect of GO is the wrapping of cells, which causes a reduction in the availability of nutrients, but also contributes to the perturbation of membranes resulting in complete cell degradation. Cell degradation and release of intracellular contents also occur due to generation of ROS, due to Van der Waals interactions between GO functional groups and cell membranes.[24,25]

Given the above facts, we hypothesize that graphene oxide provides a platform for the controlled distribution of metal nanoparticles in the proposed nanofilms, which, owing to their antibacterial properties, will harm bacterial cells by

generating ROS, which will hinder the formation of a biofilm and change its overall structure. This study aimed to create a nanofilms based on graphene oxide and silver, copper, and zinc oxide nanoparticles to prevent biofilm formation by *S. aureus, S. enterica*, and *P. aeruginosa*.

Material and Methods

Nanoparticles

Silver nanoparticles (Ag) and copper nanoparticles (Cu) were obtained from Nano-Tech (Warsaw, Poland), zinc oxide nanoparticles (ZnO; purity 99.5%) from SkySpring Nanomaterials (Houston, TX, USA), and graphene oxide (GO) from Advanced Graphene Products (Zielona Góra, Poland). Nanoparticles were diluted in ultrapure Milli-Q water (GO 5 μg/mL, Ag 25 μg/mL, Cu 12.5 μg/mL, ZnO 50 μg/mL) and sonicated at 500 W and 20 kHz for 2 min using a VC 505 Ultrasonic Liquid Processor with a cup horn (Sonics & Materials, Newtown, CT, USA); nanocomposites were left for 15 min for self-combination (physical adsorption). Thereafter, nanocomposites were centrifuged (12,000 rpm, 10 min), supernatant was discarded, and the pellets were suspended in sterile ultrapure water. Nanofilms were prepared as described above from single nanomaterials and nanocomposites (Ag 25 μg/mL + GO 5 μg/mL, Cu 12.5 μg/mL + GO 5 μg/mL, ZnO 50 μg/mL + GO 5 μg/mL) by total evaporation under sterile conditions. Similar method for nanofilms preparation was used by Pruchniewski et al 2023.[26]

Characterization of Nanomaterials

Size distribution and zeta potential were assessed for selected concentrations of nanomaterials. The nanomaterials were prepared using ultrapure water. Size distribution was evaluated by dynamic light scattering (DLS) and zeta potential by electrophoretic light scattering (ELS) with Smoluchowski approximation using a Zeta Sizer Nano-ZS90 analyzer (Malvern Instruments, Malvern, UK), in triplicate for size distribution and quadruplicate for zeta potential, at room temperature (Supplementary Materials). Both DLS and ELS are recommended methods for measuring size distribution and zeta potential, respectively.[27]

Scanning Transmission Electron Microscopy (STEM) Analysis of Nanoparticles

A drop of the suspension (approximately 5 μL) was applied to a TEM mesh made of copper foil. Then, to remove excess solution, the mesh was placed in a rotary coater chamber (POLOS Spin 150 i-NNP by SPS Semiconductor Production Systems). Thus, a thin even layer of the applied substance on the TEM mesh was obtained. The following coating parameters were used: 2000 rpm for 60s at 21°C.

After removing the mesh from the rotary coater chamber, the TEM mesh was placed in the SEM stage holder located in the scanning electron microscope chamber (Quanta 250 FEG SEM, FEI, Hillsboro, OR, USA) coupled to the scanning transmission electron microscopy detector (STEM, FEI, Hillsboro, OR, USA).[28]

Scanning Electron Microscope with Energy Dispersive X-Ray (SEM-EDX) Analysis of Nanoparticles

To perform chemical analysis of the nanocomposites using a Quanta 250 FEG FEI scanning electron microscope with an energy dispersive X-ray (SEM-EDX) detector,[28] the nanoparticle hydrocolloids were centrifuged using an MPW Centrifuge MPW-352R (10,000 rpm, 20 min) (Supplementary Materials). Then, the droplets (0.05–0.1 μL) of hydrocolloids were placed 10x on the SEM tables and dried successively in a vacuum-dried Vacucell 55 (MMM Group) at 30°C. The following parameters were used: spot 4.5, 20 kV.

Characterization of Nanofilms

The morphology and roughness of samples (GO and GO metal nanoparticles) were examined by atomic force microscopy (AFM) (NT-MDT Spectrum Instruments, Moscow, Russia). The measurements were carried out under ambient conditions in the semi-contact mode using a silicon AFM probe (NSG10/Au, NT-MDT Spectrum Instruments, Moscow, Russia) featuring a tetrahedral tip with a curvature radius of ~10 nm. The cantilever of the probe was characterized by a force constant range from 3.1 to 37.6 N/m and a resonant frequency range of 265–410 kHz. The scan size of the collected topographies was 20 μm × 20 μm with a resolution of 256 points per line. The average surface roughness (Sa)

was calculated using the Gwyddion 2.62 software (http://gwyddion.net). Similar method was performed by Olkowicz et al.[29]

Bacterial Cultures

S. aureus (ATCC 25923), *S. enterica* (ATCC 13076), and *P. aeruginosa* (ATCC 27853) were obtained from the LGC Standards (Teddington, GB). The bacterial strains were defrosted and washed three times with distilled water to purify glycerol. Thereafter, the bacteria were cultured in trypticase soy agar (TSA) (Biomaxima, Lublin, Poland) for *S. aureus* and *P. aeruginosa* and brain heart agar (BHA) (Biomaxima, Lublin, Poland) for *S. enterica* in a microbiological incubator at 37°C for 24 h.

Reactive Oxygen Species Production

The DCFDA Cellular Reactive Oxygen Species Detection Assay Kit (Abcam, Cambridge, UK) was used to measure intracellular ROS production in the bacterial cells. Fifty microliters of bacterial culture (0.5 on the McFarland scale) with DCFDA reagent (1μL/mL) were added to a 96-well plate, 50 μL of nanoparticles was added (GO 5 μg/mL, Ag 25 μg/mL, Cu 12.5 μg/mL, ZnO 50 μg/mL; nanocomplexes GO 5 μg/mL + Ag 25 μg/mL, GO 5 μg/mL + Cu 12.5 μg/mL, GO 5 μg/mL + ZnO 50 μg/mL), and the plates were incubated at 37°C protected from the light. Fluorescence was measured at excitation and emission wavelengths of 485 and 535 nm, respectively, using an ELISA reader (Infinite M200; Tecan, Durham, NC, USA). The results were expressed as the ratio between two time points: 0 and 45 min.[30]

Antioxidant Capacity

To determine antioxidant capacity, Trolox was measured using an OxiSelect™ Trolox Equivalent Antioxidant Capacity (TEAC) Assay Kit (ABTS) (Cell Biolabs Inc., San Diego, California, USA). Cell lysates were prepared according to the manufacturer's instructions. Bacterial strains were cultured in TSA for *S. aureus* and *P. aeruginosa* and in BHA for *S. enterica* at 37°C for 24 h. Thereafter, bacteria were placed in distilled saline buffer (control samples) and in nanoparticle solutions (concentrations prepared in distilled saline buffer; final concentrations: GO 5 μg/mL, Ag 25 μg/mL, Cu 12.5 μg/mL, ZnO 50 μg/mL; nanocomplexes GO 5 μg/mL + Ag 25 μg/mL, GO 5 μg/mL + Cu 12.5 μg/mL, GO 5 μg/mL + ZnO 50 μg/mL) at 37°C for 8 h. All samples were then centrifuged at 5000 *g* for 10 min, and the supernatant was collected. The test procedure was performed according to the manufacturer's instructions using standard curve dilutions. The absorbance was measured at 410 nm. The results were expressed based on a standard curve in accordance with the manual.

Biofilm Formation

Bacterial Biofilm Formation

Crystal violet staining and confocal microscopy analyses were performed to characterize the biofilm formation on the nanofilm surfaces. Crystal violet staining allowed the selection of the concentrations from which the composites were formed. Crystal violet staining is one of the basic methods for evaluation biofilm formation.[31]

For crystal violet staining, 96-well plates were covered with GO at concentrations of 2.5, 5, 10, 25, 50, and 100 μg/mL and nanoparticles (Ag, Cu, and ZnO) at concentrations of 3.125, 6.25, 12.5, 25, 50, and 100 μg/mL. Wells covered with water were used as control wells. The plates were left to completely dry under sterile conditions. Thereafter, bacterial suspensions (0.5 on the McFarland scale) were added to each well and incubated for 48 h at 37°C. After incubation, the suspensions were removed, washed 3 times with phosphate buffer saline (PBS, pH = 7.4) and fixed with methanol for 15 min. After fixation, each well was washed with PBS 3 times, and crystal violet staining was performed for 15 min. The plates were then washed five times with PBS and ethanol was added for 30 min. After the final incubation, absorbance was measured at a wavelength of 584 nm. The results are expressed as a percentage of the control sample.

For confocal microscopy analysis, nanofilms were prepared in μ-Slide 8 Well (Ibidi GmbH) in a volume of 300 μL and left for total evaporation under sterile conditions. Thereafter, 300 μL of liquid medium (tryptic soy broth for *S. aureus* and *P. aeruginosa*, brain heart infusion broth for *S. enterica*) and 10 μL of bacterial suspension (0.5 on the McFarland scale) were added into each well and incubated at 37°C for 48 h. After incubation, the medium containing the

bacteria was removed, washed three times with sterile saline buffer (pH = 7.0), fixed with methanol for 30 min, and washed with sterile saline buffer three times. To avoid non-specific staining of the biofilm structure, two dyes for nucleic acids were used. DAPI staining solution (10 µL/mL, Sigma Aldrich, Hamburg, Germany) and SYTO9 staining solution (1 µL/mL, Thermo Fisher Scientific) were added at a volume of 300 µL to each well and incubated for 30 min at room temperature protected from the light. After the staining step, the staining solutions were removed, each well was washed three times with buffer saline, and samples were placed in 90% glycerol. Each sample was analyzed using a confocal microscope (FV-1000; Olympus Corporation, Tokyo, Japan) and imaged using 60× objective lasers at 405 nm for DAPI and 488 nm for SYTO9. All images were obtained using the same laser parameters, and each sample was imaged as horizontal sample slices (Z-stack) in five fields of view. Images were analyzed using Gimp 2.10.18 software by measuring the thickness of the captured biofilm structure at five points from at least three pictures. The results are presented as the mean ± standard deviation. Examination of biofilm by confocal microscopy is a valuable tool in visualizing 3D architecture.[32]

SEM—Bacterial Biofilm Structure

Biofilm structures were analyzed by scanning electron microscopy (SEM type FEI, Quanta 200, Hillsboro, OR, USA) in low-vacuum mode at an accelerating voltage of 20 kV. Only the nanocomposites were chosen for further analysis. Nanofilms were prepared by adding 1 mL onto sterile coverslips until total evaporation under sterile conditions. Liquid medium in a volume of 1 mL and 10 µL bacterial suspension (0.5 on the McFarland scale) was placed on each coverslip and incubated at 37°C for 48 h. Thereafter, the medium with bacteria was removed, and after washing three times with sterile buffer saline, they were fixed with 2.5% glutaraldehyde for 30 min. The samples were washed three times with buffer saline, post-fixed with 1% OsO_4 in dH_2O for 30 min, and washed three times with buffer saline. Subsequently, the samples were dehydrated using a series of ethanol solutions of increasing concentrations (25% EtOH for 5 min, 50% EtOH for 5 min, 75% EtOH for 5 min, 95% EtOH for 5 min, and 100% anhydrous EtOH for 10 min). Each sample was imaged at least five times at 5000× magnification.

Statistical Analysis

All measurements are presented as mean ± standard deviation. Data were analyzed by one-way analysis of variance (ANOVA) with a post-hoc Tukey's test using GraphPad Prism 9 software (version 9.2.0, San Diego, CA, USA). Differences were considered statistically significant at p-value ≤ 0.05.

Results
Characterization of Nanomaterials and Nanofilms

Electrophoretic light scattering was used to evaluate the colloidal stability of the nanomaterials. The zeta potential values of all the samples, except ZnO, were negative (Figure 1). Metal/metal oxide nanoparticles, when combined with GO, exhibited a more negative zeta potential, even for ZnO, which reached a negative value from being initially positive. GOAg showed the most negative zeta potential value (−41.7 mV), followed by GOCu (−24.8 mV) and GOZnO (−12.2 mV). The zeta potential of the nanocomposites up to 48 h in all cases was at a constant level or became slightly more negative. Only the zeta potential of GOAg decreased to a value of −38 mV after 4 h, but began to return to its initial value after 8 h and then increased to a value of −50 mV in the following hours. The other types of nanocomposites showed more negative zeta potential values over time (Figure S1).

The size distribution of each nanomaterial exceeded 100 nm owing to the presence of GO flakes, which were visible in STEM analysis. Metal/metal oxide nanoparticles were associated with the surface of the GO flakes. Ag was evenly distributed over the surface, unlike Cu and ZnO, which formed large agglomerates that covered the entire surface of the GO flakes. The large coverage of flakes by Cu and ZnO is also evident during DLS analysis, in which those two samples showed the largest average size (437.0 nm for GOCu and 3079.7 nm for GOZnO), larger than the GO flakes themselves. A topographical analysis of the nanofilm surfaces was conducted using AFM. The addition of metal/metal oxide nanoparticles to the GO flakes caused the formed nanofilms to be characterized by increased roughness and varying
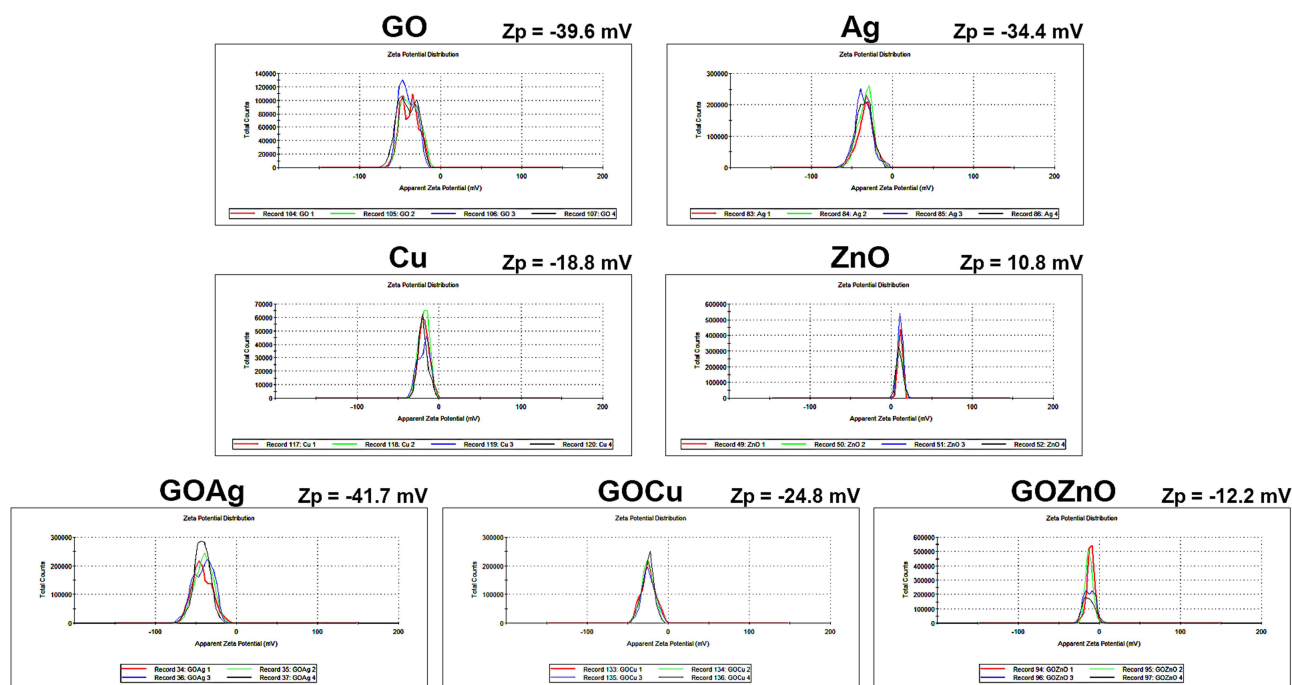
Figure 1 Zeta potentials of nanomaterials used. All measurements were performed four times. Zp is the mean value of each sample's zeta potential.

heights (Figure 2), especially when observing GOAg (Sa = 134 nm) and GOZnO (Sa = 195 nm). Interestingly, these two nanocomplexes were the most and least colloidally stable, as indicated by zeta potential analysis (Figure 1).

EDX analysis of GO and the nanocomposites showed that the spectrum of all nanomaterials consisted of signals from C and O atoms (Figure 3). The nanocomposites contained atoms typical of nanoparticles on the surface of GO. GOAg exhibited an absorption band peak for Ag at approximately 3 keV. In GOCu, the band peak corresponding to Cu was around 0.5 keV, and in GOZnO, the peak of Zn was around 1 keV. The content of the various elements found in the hydrocolloids after centrifugation is shown in Table S1. In all cases, the content of metals bound to GO was more than 99%, and residual amounts were present in the supernatant as unbound particles.

ROS Generation and Total Antioxidant Capacity

All the metal nanoparticles and nanocomposites contributed to the generation of ROS (Figure 4). For *S. aureus*, the highest level of ROS was observed in the group treated with GOAg, whereas for Gram-negative species (*S. enterica* and *P. aeruginosa*), the factor that generated the most ROS was ZnO. Antioxidant capacity was lowest in the samples treated with nanocomposites compared to the control (untreated) samples for each bacterial strain. For *S. aureus*, but no other species of bacteria tested, GO caused this value to be heightened.

Biofilm Formation

To determine the concentrations of the nanocomposites, biofilm formation from individual nanoparticles on the nanofilms was evaluated (Figure 5). The only significant concentration of GO was 5 μg/mL; however, GO was not highly toxic to the three tested bacterial species. In all species, Ag were the factor, which caused limited biofilm formation in dose-depended manner (except the lower concentration 3.125 μg/mL for *S. aureus* and *S. enterica*). Ag concentrations exceeding 25 μg/mL caused biofilm formation to a greater extent than 50%. Cu inhibited biofilm formation at similar level in the concentrations of 100 μg/mL (except *P. aeruginosa*), 50, 25, 12.5 μg/mL. Only two of the highest concentrations of ZnO (100 and 50 μg/mL) significantly reduced biofilm formation in bacteria tested.

The thickness was significantly reduced in all samples compared with that of the control probe (Figure 6). The smallest thicknesses were observed for GOAg among the three tested bacterial strains; however, the other
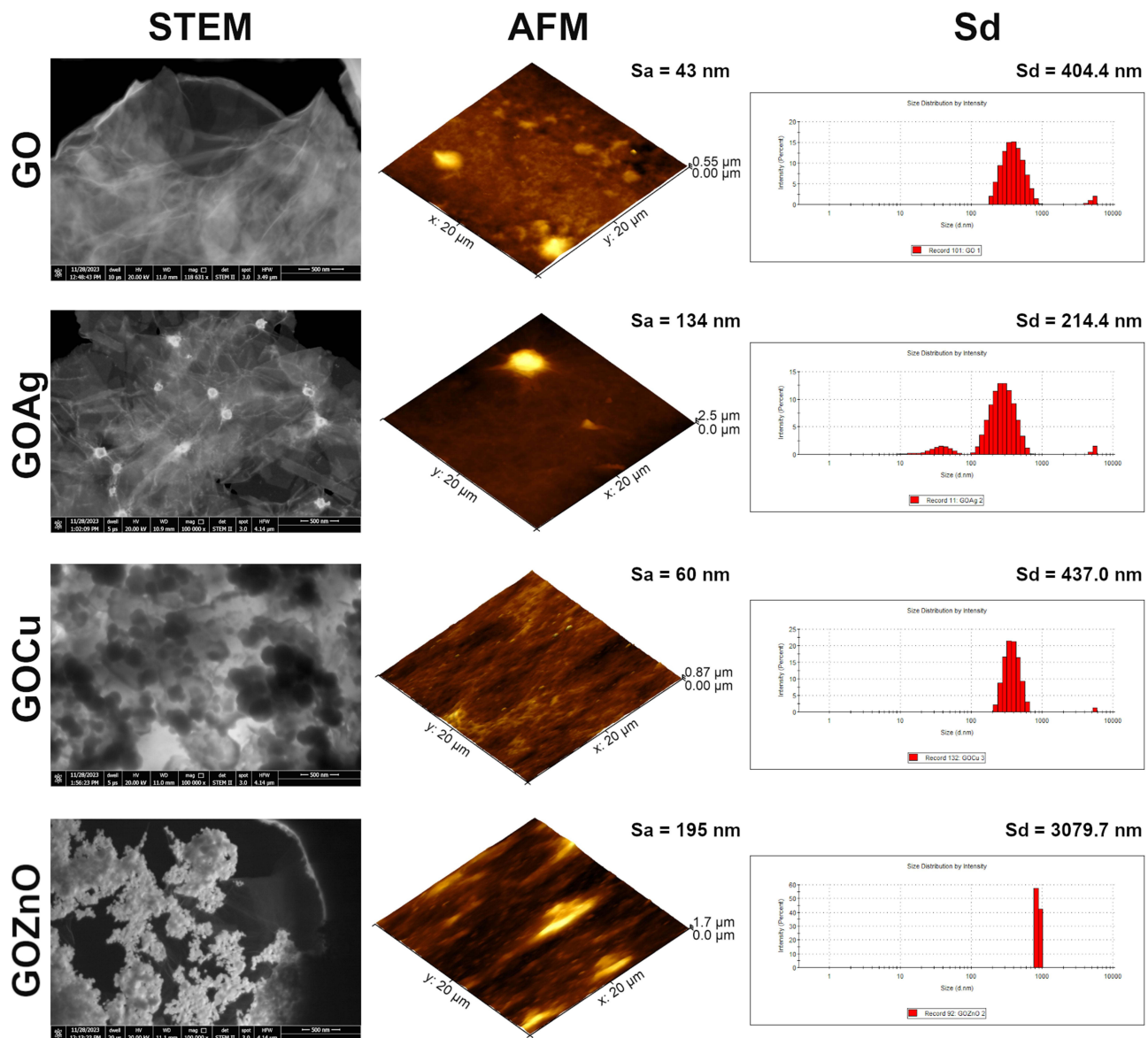
Figure 2 Physicochemical analysis of nanofilms using scanning transmission electron microscopy (STEM), atomic force microscopy (AFM), and size distribution. Sa is average surface roughness; Sd is average sample size (nm).

nanocomposites also caused a reduction in thickness and a change in the distribution of cells, which were much more loosely arranged without forming a compact layer. *P. aeruginosa* forms a biofilm with a large number of single cells that do not adhere directly to the lower layers and are located in the upper part of the biofilm. Z-stack images from which 3D views were created are shown in the Figure S2.

Visualization of the cells in the biofilm showed that the nanofilm was not favorable for creating a biofilm structure (Figure 7). *S. aureus* in the control sample (non-treated) created a spatial structure of compact cells clumped together. Many cells were observed in the GOCu and GOZnO groups although they formed significantly smaller clusters. In contrast, only a few individual cells were observed in the case of *S. aureus* and *P. aeruginosa*. *S. enterica* on the GOAg nanofilm formed a biofilm that was similar to that of the GOZnO group. Non-treated *P. aeruginosa* created a very thick and heterogeneous structure full of ECM, in which the cells were embedded, which was not observed in the test samples. The cells of all species in the control group showed proper morphology, whereas in the test groups, individual cells showed collapses in cell structure, appearing flatter, and even shrunken.
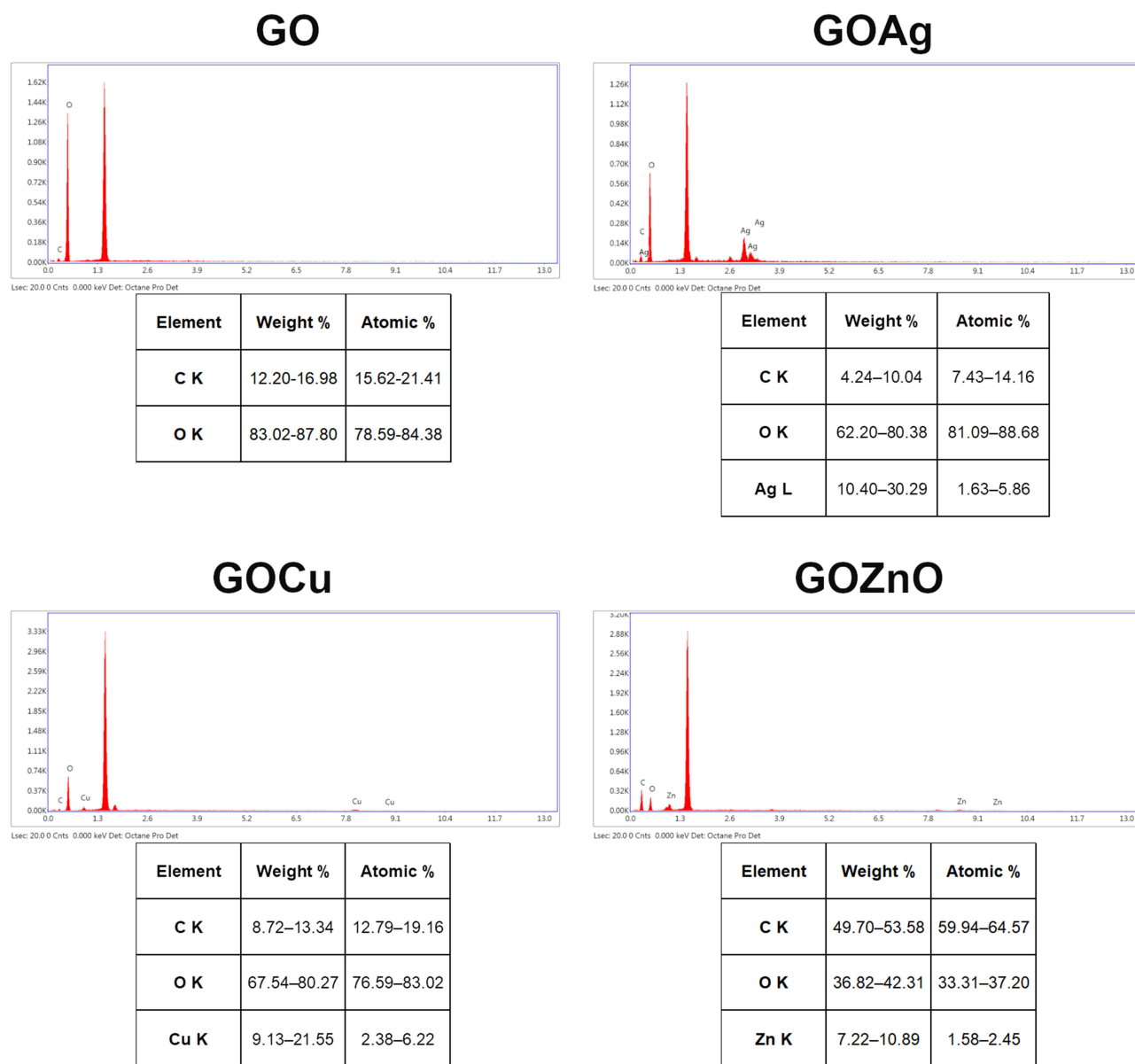
GO

Element	Weight %	Atomic %
C K	12.20-16.98	15.62-21.41
O K	83.02-87.80	78.59-84.38

GOAg

Element	Weight %	Atomic %
C K	4.24–10.04	7.43–14.16
O K	62.20–80.38	81.09–88.68
Ag L	10.40–30.29	1.63–5.86

GOCu

Element	Weight %	Atomic %
C K	8.72–13.34	12.79–19.16
O K	67.54–80.27	76.59–83.02
Cu K	9.13–21.55	2.38–6.22

GOZnO

Element	Weight %	Atomic %
C K	49.70–53.58	59.94–64.57
O K	36.82–42.31	33.31–37.20
Zn K	7.22–10.89	1.58–2.45

Figure 3 EDX analysis of GO and nanocomposites: GOAg, GOCu, GOZnO. Graphs are representative pictures. Ranges in the tables are values from at least seven spots.

Discussion

Graphene oxide is known for its electrical, optical, thermal, and mechanical properties, and metal nanomaterials exhibit special physical and chemical properties. Therefore, they can be used in a wide range of applications, from nanomedicine to optics. The decoration of GO with metal nanoparticles may provide outstanding performance in the proposed solutions, which is based on the synergistic effect these materials can demonstrate.[33] Currently, although there is research involving nanocomposites consisting of graphene oxide with metal nanoparticles, the lack of an exact mechanism of action of such nanocomposites is still highlighted, even among the latest studies.[34] The mutual change in the properties of the materials used has been demonstrated in the research presented, which is noticeable during the zeta potential analysis, in which nanocomposites were characterized by higher negative zeta potential values than the metal nanoparticles alone (Figure 1). This demonstrates the mutual stability of the two materials (GO and metal/metal oxide nanoparticles) because the zeta potential is considered a parameter indicating colloidal stability when it approaches the border value of ±30 mV. Combining materials that had negative zeta potentials with GO (−39.6 mV) increased the negative values: Ag from −34.4
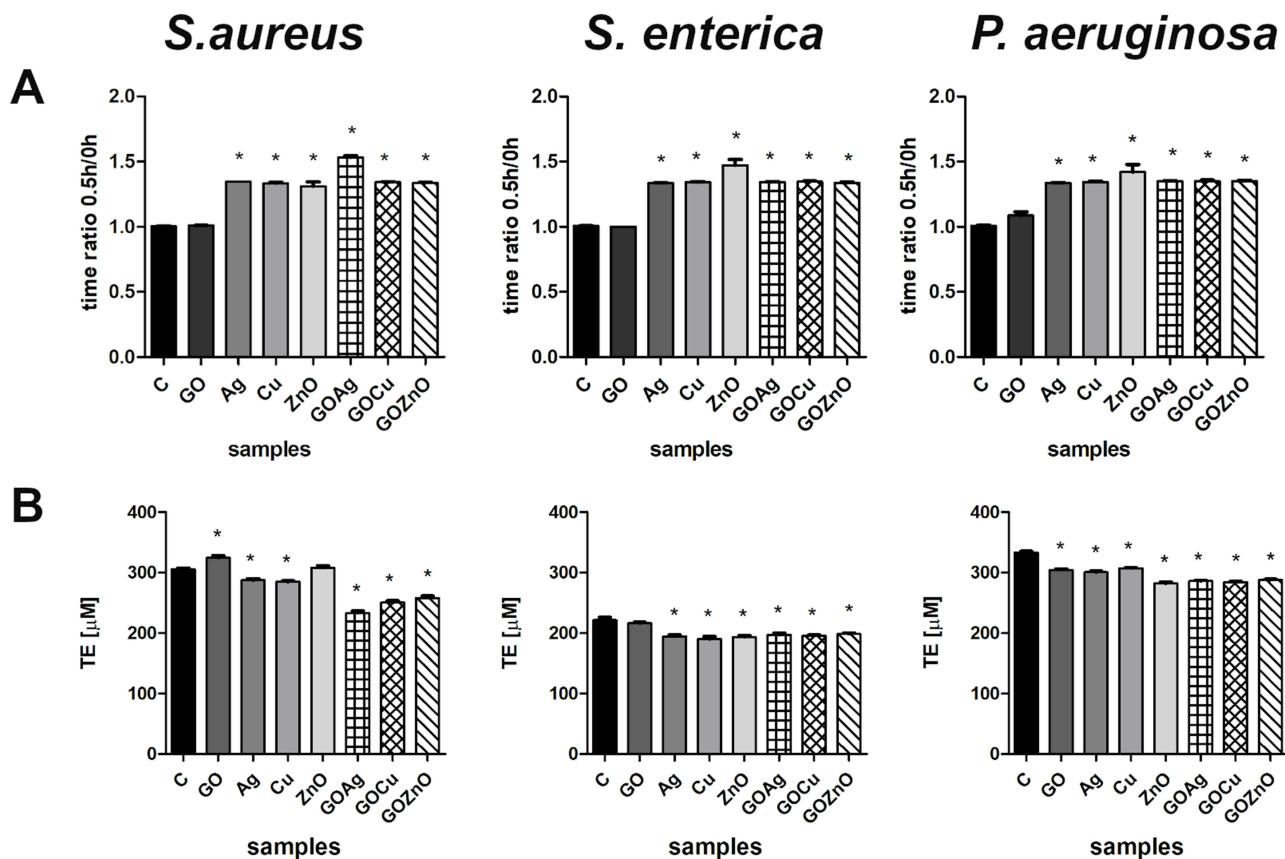
Figure 4 Generation of reactive oxygen species (ROS) (**A**) and the Trolox equivalent antioxidant capacity (TEAC) (**B**) in *S. aureus, S. enterica*, and *P. aeruginosa* after treatment with nanostructures. All results are presented as mean value ± standard deviation. *: statistically significant differences ($p \leq 0.05$) in relation to control.
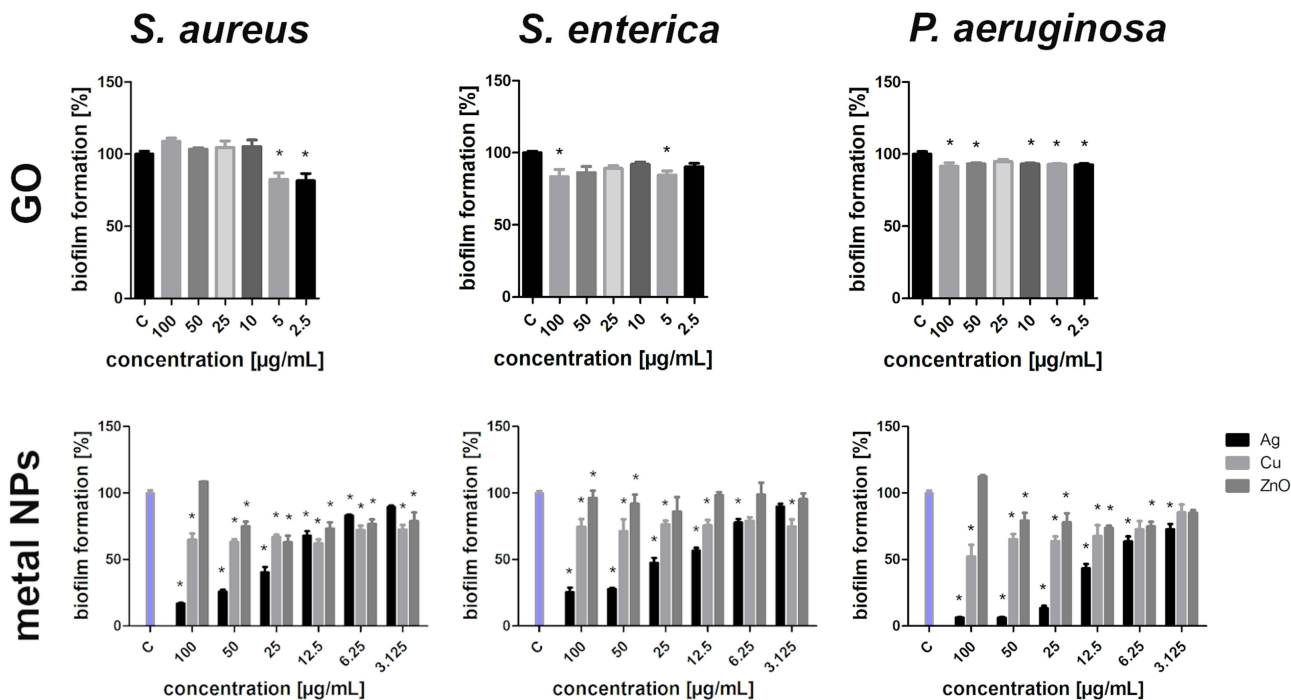

Figure 5 Biofilm formation (%) by *S. aureus, S. enterica*, and *P. aeruginosa* on the nanofilms composed of GO, Ag, Cu, and ZnO at different concentrations (µg/mL). *: statistically significant differences at $p \leq 0.05$ compared to the control samples.
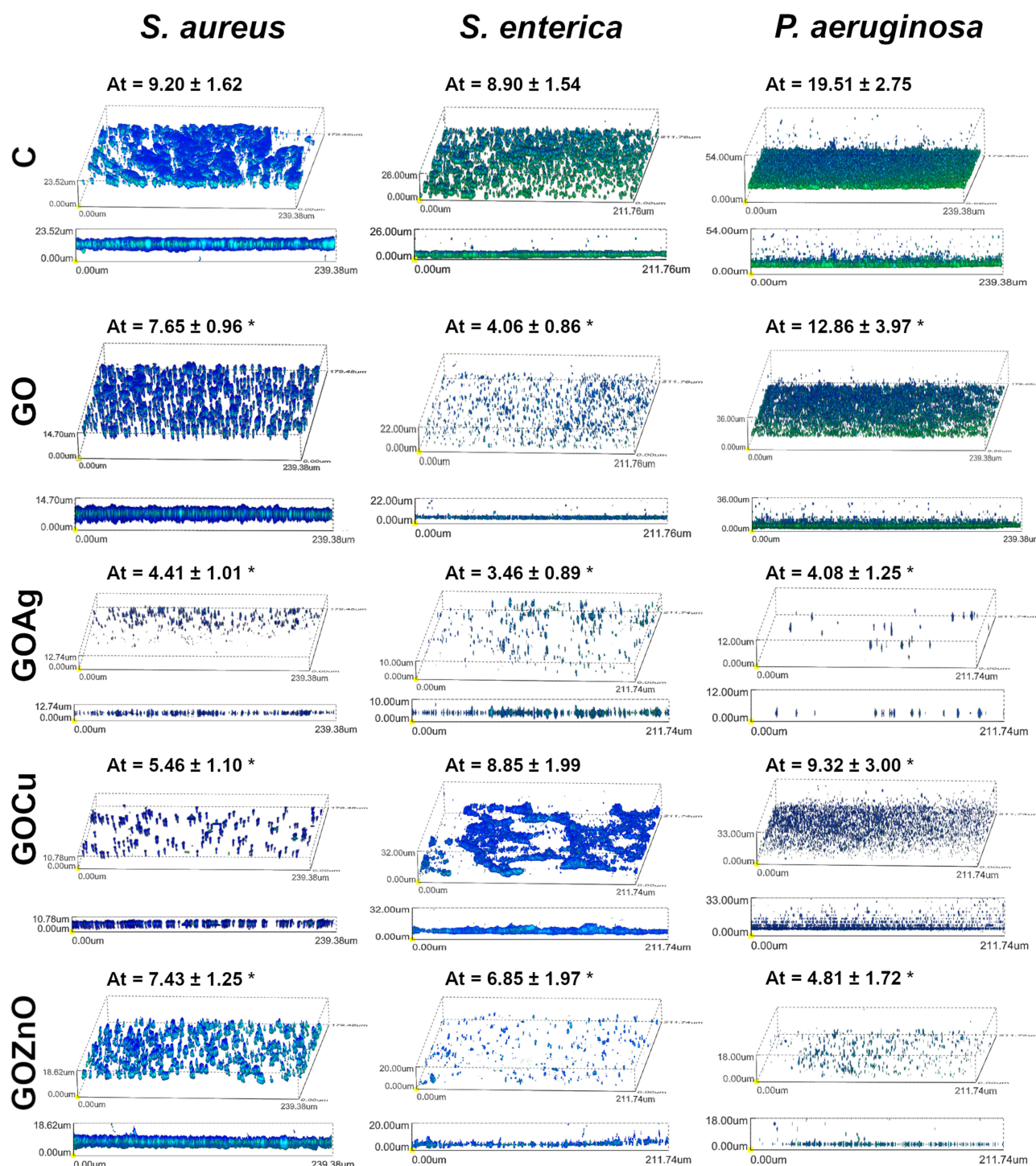
Figure 6 Confocal microscopy visualization of biofilm structure of *S. aureus, S. enterica*, and *P. aeruginosa* created on the surface of nanofilms. At is average thickness of biofilms ± standard deviation. *: statistically significant differences ($p \leq 0.05$) from the control.

mV to GOAg −41.7 mV and Cu from −18.8 mV to GOCu (−24.8 mV). The only nanoparticles with a positive zeta potential were ZnO (10.8 mV), although with GO, the value was also negative and amounted to −12.2 mV. Interestingly, the produced nanocomposites showed similar and even slightly higher stability over time up to 48h ([Figure S1]). These results are consistent with those obtained by Iravani et al, in which the GO nanocomposites also stabilized over time, increasing the zeta potential values toward higher colloidal stability.[35] The mutual action of both nanomaterials was also
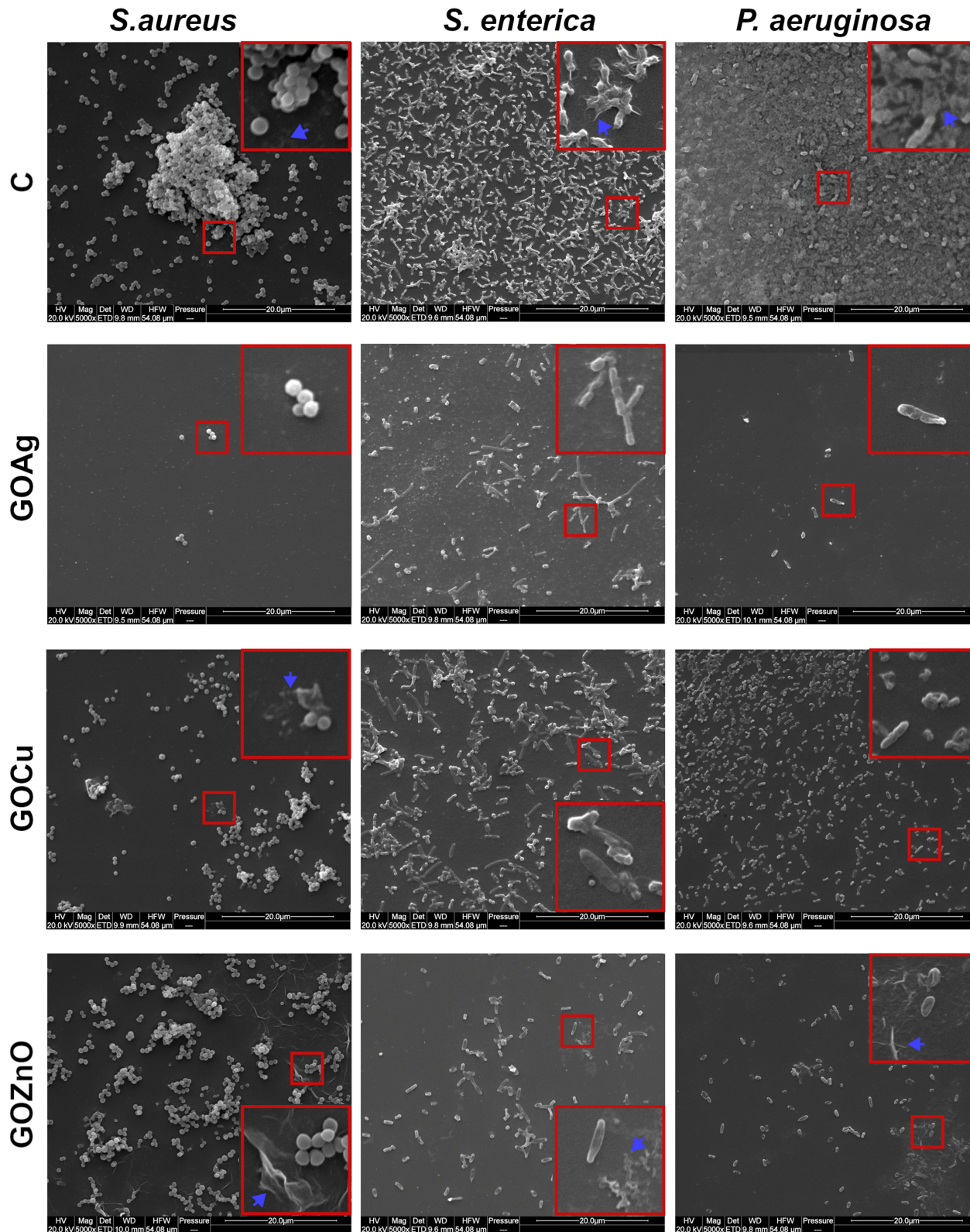
Figure 7 The biofilm structure of *S. aureus*, *S. enterica*, and *P. aeruginosa* created on the nanofilms using scanning electron microscopy with 5000× magnification. The red frames show enlarged sections. The blue arrows indicate the ECM fragments.

visible in the shape of the nanocomposite, in which GO was observed as a platform for the metal/metal oxide nanoparticles arranged on its surface (Figure 2). As GO exhibited the largest size (>400 nm) and was in the form of flakes, its nanocomposites also exhibited larger sizes owing to the arrangement of metal nanoparticles on the GO surface. Moreover, the GOZnO nanocomposite was characterized by the largest size; however, because ZnO is the least stable nanomaterial, it may have created agglomerates on GO. The formation of agglomerates (weakly bound nanoparticles) by nanoparticles with a zeta potential close to zero was also confirmed in our previous research.[36,37] This is because of the small size of individual nanoparticles, which have a high surface energy.[38] Agglomerates are relatively easy structures to overcome because the forces of interaction that occur in them are mainly electrostatic, van der Waals, solvation, or capillary effects.[39] Moreover, there are reports that larger agglomerates do not cause lower toxicity than smaller ones, which allows for further studies of even larger structures, as they may exhibit equally effective properties.[20] For this reason, the nanocomposites are larger than single nanoparticles typically exceeding 100 nm. This size of nanocomposites is consistent with the results obtained by other researchers.[28,30]

Each nanocomposite showed high carbon and oxygen contents in the samples with graphene oxide components (Figure 3). The high oxygen content of the GO group is associated with the presence of numerous oxygen-containing groups like hydroxyl, carbonyl, and epoxy groups, which are placed on the flakes made of carbon with carboxyl groups on the periphery.[40] Interestingly, GOZnO had the lowest oxygen content compared to other nanowires that were not oxides but metals themselves, yet these results are consistent with other studies that have proven that ZnO located on GO sheets can cause oxygen defects in their structure.[41] An optical absorption band peak around 3 keV is typical for Ag nanocrystallites.[42] Similar peaks around <1 keV and around 8 keV for Cu were observed by Guzman et al.[43] The metal element content of the supernatant-to-pellet comparison (nanocomposites produced) showed that all types of metal nanoparticles bound to graphene oxide at a minimum of 99% (Table S1).

It was previously demonstrated that metal nanoparticles are uniformly distributed over the surface of graphene materials, which avoids the re-deposition of graphene.[44] This phenomenon also explains the surface roughness of the nanocomposites. The surfaces of the nanocomposites were characterized by a greater surface roughness than that of bare GO (Figure 2). The surface roughness of GOZnO was 195 nm; however, as mentioned before, it was the least stable nanocomposite forming agglomerates. GOAg had the second-highest surface roughness, with an average value of 134 nm. This is consistent with the results obtained by Ahmad et al, in which silver nanoparticles were shown to decorate wrinkled graphene oxide sheets on the basis of AFM and SEM analysis.[45] However, rough surfaces are more suitable for bacterial adhesion than smooth surfaces because of the increased surface area and protection against external forces.[46] Depending on the stimuli provided by the environment, bacterial cells promote the transcription of genes responsible for the transition from planktonic forms to cells adjacent to the surface. Interactions of cells with each other as well as cells with the surface therefore play an important role in biofilm formation. In a study conducted by Yadav et al it has been shown that its presence can interfere with any of these processes, helping to reduce biofilm formation.[47] In our study, all types of nanocomposites contained GO, albeit they were doped with metal nanoparticles, which further affected their properties.

All nanocomposites caused generation of reactive oxygen species (statistically significant) (Figure 4). For *S. aureus*, GOAg was the causative agent of ROS formation to the greatest extent, while for Gram-negative bacteria it was ZnO. However, the antibacterial properties of ZnO are mainly attributed to membrane disruption or generation of intracellular ROS. It is also believed that zinc oxide nanoparticles' morphology affects their interaction with bacterial cells.[48] In our studies, ZnO was one of the least colloidally stable nanoparticles; thus, these nanoparticles created agglomerates which restricted direct contact with the bacterial surface. In general, ROS generation is one of the main cytotoxic factors during in vitro studies following exposure to NPs. Therefore, it is believed that metal-based nanoparticles act on the bacterial membrane by releasing ions, and this is proposed as a main antibacterial mechanism.[49] The generation of oxidative stress in bacteria may result from the disruption of the electron transport chain due to the high affinity of silver nanoparticles for the cell membrane.[50] In our study, nanocomposites interact with cell membrane (which is evident in SEM analysis in our study due to the presence of cells with changed structures). Cell membrane is responsible for electron chain transfer. Molecular oxygen produces O2•, which is the primary ROS by one-electron reduction catalyzed by nicotinamide adenine dinucleotide phosphate (NADPH) oxidase. Further reduction of molecular oxygen may lead to forming either H2O2 or

OH•, via dismutation and metal-catalyzed Fenton reaction via dismutation and metal-catalyzed Fenton reaction. Nevertheless, the exact mechanism of ROS-mediated antibacterial action of nanoparticles (eg AgNPs) is not fully clear.[51] Gram-negative cell structures are characterized by an outer membrane (OM) and thin cell wall. As the cell membrane is the cover and barrier between the cell interior and external environment, it represents the first point of direct contact between nanoparticles and bacterial cells. In contrast to typical biological membranes, OM is permeable to small, water-soluble molecules.[52] As shown by Yusof et al,[53] zinc oxide nanoparticles realize zinc ions in parallel with incubation time. ZnO generates ROS because of its electronic band structure. GOCu contributed similar levels of ROS to other nanocomposites, which suggests an effective action; however, this was not observed in the biofilm analysis (Figures 6 and 7), where GOCu appeared to be the least toxic. Similarly, the biofilm formed on its base was the thickest and had the highest number of cells, which indicates that GOCu is effective for planktonic forms, but not for biofilms. One of the proposed mechanisms of copper nanoparticles is the release of ions that, among other things, interact with cells by inhibiting the production of enzymes and proteins but also have a high affinity for amines and carboxyl groups found on the surface of cells, allowing direct binding to cells.[54] This could explain the results obtained, since the cells in the biofilm are nested in an ECM. Even if some materials do not show a reduction in biofilm formation in crystal violet staining (such as bare GO, ZnO, and some concentrations of Cu and Ag) (Figure 5), there are some ways to overcome this and improve their toxicity. For example, the antibacterial efficiency of ZnO nanoparticles toward both Gram-positive and Gram-negative species can be increased by combining them with carbon materials, particularly GO. Thus, it is possible to increase the efficiency by up to two times compared with single nanoparticles.[55]

Antioxidant capacity is the ability to scavenge free radicals.[56] If the nanocomposites produce ROS, this capacity is reduced, as can be seen in the present study (Figure 4). Interestingly, in Gram-negative bacteria, all metal nanoparticles and nanocomposites caused an increase in ROS and a decrease in antioxidant capacity, whereas in Gram-positive bacteria such as *S. aureus*, similar results were observed in the extent of ROS production, but no similar relationship was observed when analyzing antioxidant capacity. Although these results do not show a clear relationship in all groups, according to Metryka et al, nanoparticles' antioxidant capacity may be connected with down-regulation of the genes encoding antioxidants, which are, in turn, related to increased regulation of genes involved in repairing bacterial outer layers, nucleic acids, and other genes responsible for cell homeostasis.[57] Such a mechanism seems probable, especially as in our studies, the bacterial cells had defects in their outer layers, which is visible in SEM analysis. Moreover, metal nanoparticles may inhibit antioxidant enzymes (eg SO, CAT) because of altering their secondary structure, which in consequence cannot function properly. Antioxidant capacity is the summary activity of cells' components, which protect from oxidative stress and free radicals produced.[58] It means that during exposure to metal nanoparticles, antioxidant enzymes show no or lesser activity due to change in their structure. In study presented, the antioxidant capacity was lower in case of nanocomposites than in the control sample (not treated with nanocomposite/nanoparticles), meaning that total antioxidant activity was lowered than properly functioning cells (control group).

The changes caused by the nanocomposite base also contributed to a reduction in the thickness of the resulting biofilm (Figure 6), which indicates not only the degradation of individual cells but also the destruction of the entire structure. However, only cells were stained during biofilm analysis, with no separate staining of the extracellular matrix. In the control groups, the interconnected cells formed a multilayer structure, as shown in z-stack images in Figure S2. The transport of nanoparticles within the biofilm structure may be affected by the presence of water channels, which makes it possible for nanoparticles to reach deeper layers. Such a phenomenon is desirable because it ensures not only the degradation of cells in the upper layers but also the destruction of the structure from within, where the cells exhibit other metabolic properties. In the present study, this may have been the case with nanocomposites decorated with metal nanoparticles, which was partially confirmed by confocal microscopy analysis (Figure 6), where the entire biofilm structure was degraded, and the cells were arranged in a thinner layer. In addition, their arrangement changed when treated with nanocomposites, especially GOAg, forming a much less layered structure (Figure S2). However, the migration of nanoparticles is desirable when their transport occurs through channels, whereas in the biofilm structure, there are structures called pores. Antibacterial agents are diluted within the pores, which can weaken their effect.[14] The test results do not indicate the accumulation of nanoparticles in the pores. However, because of the constant reorganization of the biofilm structure, this cannot be excluded during prolonged exposure.

Nevertheless, the obtained results were confirmed by SEM analysis (Figure 7), in which the cells were further apart, and EPS was partially degraded, although small fragments of the matrix were visible in the treated groups. The lowest cell density was observed for the GOAg and GOZnO groups. Interestingly, the two types of films exhibited the highest average surface roughness values. These results are consistent with other research findings by Wu et al, which indicated that rough surfaces reduced the number of viable bacterial cells (*S. aureus* and *P. aeruginosa* were used as bacterial models) after only 4 h in the early stages of biofilm formation.[59] In other research, rougher surfaces of ZnO contributed to less metabolic activity and, consequently, to a decrease in bacterial viability in comparison to smooth surfaces.[60] These results suggest that even though rough surfaces are generally considered more attractive for bacterial cell adhesion, they are not conducive to biofilm formation, but only when planktonic forms settle on nanofilms. This may be related to the long distances between bacteria when they inhabit rough surfaces, making them unable to form a three-dimensional structure through their inability to communicate via quorum sensing based on chemical signals, which informs them about population density, transfer of genetic material, or synthesis of secondary metabolites.[61]

GOAg despite its rough surface, was the most limiting factor for biofilm formation by all species tested, which was visible during biofilm analysis (Figures 6 and 7). Silver nanoparticles are well known for their antibacterial properties owing to ion realization, which, among other things, can adhere to cell walls and membranes and interrupt envelope structures.[62] This may also explain why the bacterial cells were deformed when exposed to the nanocomposites, as was evident from the SEM analysis (Figure 7). Jang et al also demonstrated the great potential of the GOAg nanocomposite, which significantly inhibited Gram-positive bacteria exemplified by *S. epidermidis* and to a lesser extent Gram-negative bacteria *P. aeruginosa*.[63] Codita et al[64] documented that nanofilms composed of silver and copper had strong antibacterial properties against both Gram-positive and Gram-negative species, although this depended on the physicochemical properties of these nanofilms.

Summarizing the effect of the nanocomposites, GOAg was the most effective against all three bacterial strains (*S. aureus, S. enterica* and *P. aeruginosa*). It was the agent with the highest colloidal stability (zeta potential of −41.7 mV), and thus the lowest tendency to agglomerate, which can also be seen in the expressed hydrodynamic diameter of 214.4 nm. The nanocomposites had a high average surface roughness (Sa = 134 nm), but due to their high toxicity, this was not a parameter promoting biofilm formation. For Gram-positive bacteria, using *S. aureus* as an example, this was the factor generating the highest amount of ROS formation, as well as reducing the total antioxidant capacity of the bacteria to the greatest extent. Exposure of all three tested bacterial species to GOAg resulted in the greatest reduction in biofilm thickness based on cell alignment. A significantly degraded biofilm structure is also observed during SEM analysis, in which *S. aureus* and *P. aeruginosa* were characterized by the presence of only a few cells.

The GOCu nanocomposite had medium colloidal stability, with a zeta potential of −24.8 mV. The nanocomposites had the lowest surface roughness among the types of nanocomposites analyzed (Sa = 60 nm) and a larger hydrodynamic diameter than GOAg (437.0 nm). The nanocomposite caused ROS generation at a similar level to GOZnO in *S. aureus*, and for the other two bacterial species at a similar level to all nanocomposites used, although these results are statistically significant. GOCu also inhibited biofilm structure for two bacterial species (*S. aureus* and *P. aeruginosa*), although a lower number of *S. enterica* cells were apparent on SEM analysis compared to the control group (results not statistically significant on analysis by confocal microscopy).

GOZnO nanocomposites were characterized by the lowest colloidal stability (zeta potential equal to −12.2 mV), and thus the highest hydrodynamic diameter and the highest surface roughness, due to the formation of agglomerates. Nevertheless, it was a factor that statistically significantly caused ROS generation and reduced total antioxidant capacity in all tested bacterial species. In addition, it significantly reduced the cell content of the biofilm, although to the greatest extent in *P. aeruginosa*.

Conclusion

These results make it possible to select an effective antimicrobial agent that can reduce biofilm formation. The combination of metal nanoparticles with graphene oxide, which constitutes a platform and improves the physicochemical properties of metal nanoparticles, is effective as a film that limits biofilm formation, resulting in changes in both the biofilm architecture and the thickness of the overall structure. This is particularly important, as biofilms are a real threat

to public health; however, owing to their complex structure, they are difficult to eradicate and can persist despite the use of conventional antibacterial agents.

In conclusion, the nanocomposites prepared as presented resulted in significant binding of metal nanoparticles to graphene oxide. In addition, all nanocomposites remained stable after 48h, which is particularly important for long-term applications such as coating materials associated with medical-related fields or food packaging, among others. These results therefore contribute to the possibility of developing coating technologies for such surfaces that will reduce biofilm formation in a controlled manner.

Acknowledgments

Funding

Disclosure
The author(s) report no conflicts of interest in this work.

References

1. Berlanga M, Guerrero R. Living together in biofilms: the microbial cell factory and its biotechnological implications. *Microb Cell Fact*. 2016;15 (1):1–11. doi:10.1186/S12934-016-0569-5/FIGURES/3
2. Toyofuku M, Inaba T, Kiyokawa T, Obana N, Yawata Y, Nomura N. Environmental factors that shape biofilm formation. *Biosci Biotechnol Biochem*. 2016;80(1):7–12. doi:10.1080/09168451.2015.1058701
3. Flemming HC, Neu TR, Wozniak DJ. The EPS matrix: the "House of Biofilm Cells. *J Bacteriol*. 2007;189(22):7945–7947. doi:10.1128/JB.00858-07
4. Pinto RM, Soares FA, Reis S, Nunes C, Van Dijck P. Innovative Strategies Toward the Disassembly of the EPS Matrix in Bacterial Biofilms. *Front Microbiol*. 2020;11(May):1–20. doi:10.3389/fmicb.2020.00952
5. Mirzaei R, Mohammadzadeh R, Alikhani MY, et al. The biofilm-associated bacterial infections unrelated to indwelling devices. *IUBMB Life*. 2020;72(7):1271–1285. doi:10.1002/IUB.2266
6. Khatoon Z, McTiernan CD, Suuronen EJ, Mah TF, Alarcon EI. Bacterial biofilm formation on implantable devices and approaches to its treatment and prevention. *Heliyon*. 2018;4(12):e01067. doi:10.1016/J.HELIYON.2018.E01067
7. Archer NK, Mazaitis MJ, William Costerton J, Leid JG, Powers ME, Shirtliff ME. Staphylococcus aureus biofilms: properties, regulation and roles in human disease. *Virulence*. 2011;2(5):445. doi:10.4161/VIRU.2.5.17724
8. Thi MTT, Wibowo D, Rehm BHA. Pseudomonas aeruginosa Biofilms. *Int J Mol Sci*. 2020;21(22):8671. doi:10.3390/IJMS21228671
9. Harrell JE, Hahn MM, D'Souza SJ, et al. Salmonella Biofilm Formation, Chronic Infection, and Immunity Within the Intestine and Hepatobiliary Tract. *Front Cell Infect Microbiol*. 2021;10:624622. doi:10.3389/FCIMB.2020.624622
10. Subhadra B, Gondil VS. *E D I to R I a L Open Access Biofilms and Their Role on Diseases*. doi:10.1186/s12866-023-02954-2
11. Lin YK, Yang SC, Hsu CY, Sung JT, Fang JY. The Antibiofilm Nanosystems for Improved Infection Inhibition of Microbes in Skin. *Molecules*. 2021;26(21):6392. doi:10.3390/MOLECULES26216392
12. Gomaa HH, Amin DY, Ahmed AR, Ismail NA, El Dougdoug KA, Abd-Elhalim BT. Antimicrobial, antibiofilm, and antiviral investigations using Egyptian Phoenix dactylifera L. pits extract. *AMB Express*. 2024;14(1):1–11. doi:10.1186/S13568-024-01695-3/FIGURES/3
13. Shkodenko L, Kassirov I, Koshel E. Metal Oxide Nanoparticles Against Bacterial Biofilms: perspectives and Limitations. *Microorganisms*. 2020;8 (10):1545. doi:10.3390/microorganisms8101545
14. Quan K, Hou J, Zhang Z, et al. Water in bacterial biofilms: pores and channels, storage and transport functions. *Crit Rev Microbiol*. 2022;48 (3):283–302. doi:10.1080/1040841X.2021.1962802
15. Balaure PC, Grumezescu AM. Recent Advances in Surface Nanoengineering for Biofilm Prevention and Control. Part I: molecular Basis of Biofilm Recalcitrance. Passive Anti-Biofouling Nanocoatings. *Nanomaterials*. 2020;10(6):1–30. doi:10.3390/NANO10061230
16. Hosnedlova B, Kabanov D, Kepinska M, et al. Effect of Biosynthesized Silver Nanoparticles on Bacterial Biofilm Changes in S aureus and E. coli. *Nanomaterials*. 2022;12(13):2183. doi:10.3390/NANO12132183
17. Franco D, Calabrese G, Guglielmino SPP, Conoci S. Metal-Based Nanoparticles: antibacterial Mechanisms and Biomedical Application. *Microorganisms*. 2022;10(9):1778. doi:10.3390/MICROORGANISMS10091778
18. Li H, Yang Z, Khan SA, Walsh LJ, Seneviratne CJ, Ziora ZM. Characteristics of Metallic Nanoparticles (Especially Silver Nanoparticles) as Anti-Biofilm Agents. *Antibiotics*. 2024;13(9):819. doi:10.3390/ANTIBIOTICS13090819
19. Abdelhai MF, Shabaan RH, Kamal NM, Elemary EA, Abd-Elhalim BT, Hassan EA. Copper nanoparticles biosynthesis by Stevia rebaudiana extract: biocompatibility and antimicrobial application. *AMB Express*. 2024;14(1):1–15. doi:10.1186/S13568-024-01707-2/TABLES/4
20. Zhang N, Xiong G, Liu Z. Toxicity of metal-based nanoparticles: challenges in the nano era. *Front Bioeng Biotechnol*. 2022;10:1001572. doi:10.3389/FBIOE.2022.1001572/BIBTEX
21. Yin PT, Shah S, Chhowalla M, Lee KB. Design, synthesis, and characterization of graphene-nanoparticle hybrid materials for bioapplications. *Chem Rev*. 2015;115(7):2483–2531. doi:10.1021/CR500537T

22. Kumar B, Kumar B. Graphene- and Graphene Oxide-Bounded Metal Nanocomposite for Remediation of Organic Pollutants. *Carbon-Based Mater Environ Protect Remediat.* 2020. doi:10.5772/INTECHOPEN.92992

23. Parnianchi F, Nazari M, Maleki J, Mohebi M. Combination of graphene and graphene oxide with metal and metal oxide nanoparticles in fabrication of electrochemical enzymatic biosensors. *Int Nano Lett.* 2018;8(4):229–239. doi:10.1007/S40089-018-0253-3

24. Saeed SI, Vivian L, CWSCW Z, et al. Antimicrobial activities of graphene oxide against biofilm and intracellular Staphylococcus aureus isolated from bovine mastitis. *BMC Vet Res.* 2023;19(1):1–11. doi:10.1186/S12917-022-03560-6/FIGURES/8

25. Ravikumar V, Mijakovic I, Pandit S. Antimicrobial Activity of Graphene Oxide Contributes to Alteration of Key Stress-Related and Membrane Bound Proteins. *Int J Nanomed.* 2022;17:6707. doi:10.2147/IJN.S387590

26. Pruchniewski M, Sawosz E, Sosnowska-Ławnicka M, et al. Nanostructured graphene oxide enriched with metallic nanoparticles as a biointerface to enhance cell adhesion through mechanosensory modifications. *Nanoscale.* 2023;15(46):18639–18659. doi:10.1039/D3NR03581F

27. Garg S, Patel P, Gupta GD, Kurmi BD. Pharmaceutical Applications and Advances with Zetasizer: an Essential Analytical Tool for Size and Zeta Potential Analysis. *Micro Nanosyst.* 2024;16(3):139–154. doi:10.2174/0118764029301470240603051432

28. Zielińska-Górska M, Sosnowska-ławnicka M, Jaworski S, et al. Silver Nanoparticles and Graphene Oxide Complex as an Anti-Inflammatory Biocompatible Liquid Nano-Dressing for Skin Infected with Staphylococcus aureus. *J Inflamm Res.* 2023;16:5477. doi:10.2147/JIR.S431565

29. Olkowicz K, Kowalczyk K, Buczko Z, Czwartos J, Nasiłowska B. Durability and Additional Properties of Anodized Aluminum-Based Coatings with Different Wettability under Natural Conditions. *Materials.* 2023;16(10):3729. doi:10.3390/MA16103729/S1

30. Jaworski S, Wierzbicki M, Sawosz E, et al. Graphene oxide-based nanocomposites decorated with silver nanoparticles as an antibacterial agent. *Nanoscale Res Lett.* 2018;13(1):1–17. doi:10.1186/S11671-018-2533-2/FIGURES/13

31. Borowicz M, Krzyżanowska DM, Jafra S. Crystal violet-based assay for the assessment of bacterial biofilm formation in medical tubing. *J Microbiol Methods.* 2023;204:106656. doi:10.1016/J.MIMET.2022.106656

32. Mountcastle SE, Vyas N, Villapun VM, et al. Biofilm viability checker: an open-source tool for automated biofilm viability analysis from confocal microscopy images. *npj Biofilms Microb.* 2021;7(1):1–12. doi:10.1038/s41522-021-00214-7

33. Iordache M, Oubraham A, Sorlei IS, et al. Noble Metals Functionalized on Graphene Oxide Obtained by Different Methods—New Catalytic Materials. *Nanomaterials.* 2023;13(4):783. doi:10.3390/NANO13040783

34. Badoni A, Prakash J. Noble metal nanoparticles and graphene oxide based hybrid nanostructures for antibacterial applications: recent advances, synergistic antibacterial activities, and mechanistic approaches. *Micro Nano Eng.* 2024;22:100239. doi:10.1016/J.MNE.2024.100239

35. Iravani M, Simjoo M, Chahardowli M, Moghaddam AR. Experimental insights into the stability of graphene oxide nanosheet and polymer hybrid coupled by ANOVA statistical analysis. *Sci Rep.* 2024;14(1):1–18. doi:10.1038/s41598-024-68218-9

36. Lange A, Sawosz E, Wierzbicki M, et al. Nanocomposites of Graphene Oxide—Silver Nanoparticles for Enhanced Antibacterial Activity: mechanism of Action and Medical Textiles Coating. *Materials.* 2022;15(9):3122. doi:10.3390/MA15093122

37. Lange A, Sawosz E, Daniluk K, et al. Bacterial Surface Disturbances Affecting Cell Function during Exposure to Three-Compound Nanocomposites Based on Graphene Materials. *Nanomaterials.* 2022;12(17):3058. doi:10.3390/NANO12173058/S1

38. Shrestha S, Wang B, Dutta P. Nanoparticle processing: understanding and controlling aggregation. *Adv Colloid Interface Sci.* 2020;279:102162. doi:10.1016/j.cis.2020.102162

39. Endres SC, Ciacchi LC, Mädler L. A review of contact force models between nanoparticles in agglomerates, aggregates, and films. *J Aerosol Sci.* 2021;153:105719. doi:10.1016/J.JAEROSCI.2020.105719

40. Uflyand IE, Naumkina VN, Zhinzhilo VA. Nanocomposites of Graphene Oxide and Metal-Organic Frameworks. *Russ J Appl Chem.* 2021;94 (11):1453–1468. doi:10.1134/S107042722111001X/FIGURES/9

41. TDH L, Tuan HNA, Trinh KS, Van KT. Enhanced antibacterial property of zinc oxide nanoparticles by incorporation of graphene oxide. *J Sol-Gel Sci Technol.* 2022;104(1):246–257. doi:10.1007/S10971-022-05923-9

42. Safaepour M, Shahverdi AR, Shahverdi HR, Khorramizadeh MR, Gohari AR. Green Synthesis of Small Silver Nanoparticles Using Geraniol and Its Cytotoxicity against Fibrosarcoma-Wehi 164. *Avicenna J Med Biotechnol.* 2009;1(2):111–115.

43. Guzman M, Arcos M, Dille J, Godet S, Rousse C. Effect of the concentration of NaBH4 and N2H4 as reductant agent on the synthesis of copper oxide nanoparticles and its potential antimicrobial applications. *Nano Biomed Eng.* 2018;10(4):392–405. doi:10.5101/NBE.V10I4.P392-405

44. Moafi A, Heidari O, Soltannia B, Wlodarski W, Shahi F, Parvin P. Reduction of metal nanoparticle decorated flexible graphene oxide by laser at various temperatures and under selected atmospheres. *Carbon Trends.* 2022;6:100140. doi:10.1016/J.CARTRE.2021.100140

45. Ahmad MA, Aslam S, Mustafa F, Arshad U. Synergistic antibacterial activity of surfactant free Ag–GO nanocomposites. *Sci Rep.* 2021;11(1):196. doi:10.1038/s41598-020-80013-w

46. Schubert A, Griesmüller C, Gersdorff N, Bürgers R, Wiechens B, Wassmann T. Antibacterial coating of orthodontic elastomeric ligatures with silver and bismuth nanofilms by magnetron sputtering: a feasibility study. *Clin Exp Dent Res.* 2024;10(2). doi:10.1002/CRE2.864

47. Yadav N, Dubey A, Shukla S, et al. Graphene Oxide-Coated Surface: inhibition of Bacterial Biofilm Formation due to Specific Surface-Interface Interactions. *ACS Omega.* 2017;2(7):3070–3082. doi:10.1021/ACSOMEGA.7B00371/SUPPL_FILE/AO7B00371_SI_001.PDF

48. Singh R, Cheng S, Singh S. Oxidative stress-mediated genotoxic effect of zinc oxide nanoparticles on Deinococcus radiodurans. *3 Biotech.* 2020;10 (2):1–13. doi:10.1007/S13205-020-2054-4/TABLES/1

49. Alavi M, Rai M, Martinez F, et al. The efficiency of metal, metal oxide, and metalloid nanoparticles against cancer cells and bacterial pathogens: different mechanisms of action. *Cellular Molecular Biomed Rep.* 2022;2(1):10–21. doi:10.55705/cmbr.2022.147090.1023

50. Quinteros MA, Cano Aristizábal V, Dalmasso PR, Paraje MG, Páez PL. Oxidative stress generation of silver nanoparticles in three bacterial genera and its relationship with the antimicrobial activity. *Toxicol in vitro.* 2016;36:216–223. doi:10.1016/J.TIV.2016.08.007

51. Dakal TC, Kumar A, Majumdar RS, Yadav V. Mechanistic basis of antimicrobial actions of silver nanoparticles. *Front Microbiol.* 2016;7 (NOV):231711. doi:10.3389/FMICB.2016.01831/BIBTEX

52. Sun J, Rutherford ST, Silhavy TJ, Huang KC. Physical properties of the bacterial outer membrane. *Nat Rev Microbiol.* 2022;20(4):236. doi:10.1038/S41579-021-00638-0

53. Mohd Yusof H, Abdul Rahman N, Mohamad R, Hasanah Zaidan U, Samsudin AA. Antibacterial potential of biosynthesized zinc oxide nanoparticles against poultry-associated foodborne pathogens: an in vitro study. *Animals.* 2021;11(7):2093. doi:10.3390/ani11072093

54. Kim J, Kang SH, Choi Y, et al. Antibacterial and biofilm-inhibiting cotton fabrics decorated with copper nanoparticles grown on graphene nanosheets. *Sci Rep.* 2023;13(1):1–11. doi:10.1038/s41598-023-38723-4

55. Gudkov SV, Burmistrov DE, Serov DA, Rebezov MB, Semenova AA, Lisitsyn AB. A Mini Review of Antibacterial Properties of ZnO Nanoparticles. *Front Phys*. 2021;9:49. doi:10.3389/fphy.2021.641481

56. Bedlovičová Z, Strapáč I, Baláž M, Salayová A. A Brief Overview on Antioxidant Activity Determination of Silver Nanoparticles. *Molecules*. 2020;25(14):3191. doi:10.3390/MOLECULES25143191

57. Metryka O, Wasilkowski D, Mrozik A. Evaluation of the Effects of Ag, Cu, ZnO and TiO2 Nanoparticles on the Expression Level of Oxidative Stress-Related Genes and the Activity of Antioxidant Enzymes in Escherichia coli, Bacillus cereus and Staphylococcus epidermidis. *Int J Mol Sci*. 2022;23(9):4966. doi:10.3390/IJMS23094966/S1

58. Liu W, Worms I, Slaveykova VI. Interaction of silver nanoparticles with antioxidant enzymes. *Environ Sci Nano*. 2020;7(5):1507–1517. doi:10.1039/C9EN01284B

59. Wu S, Altenried S, Zogg A, Zuber F, Maniura-Weber K, Ren Q. Role of the Surface Nanoscale Roughness of Stainless Steel on Bacterial Adhesion and Microcolony Formation. *ACS Omega*. 2018;3(6):6456–6464. doi:10.1021/ACSOMEGA.8B00769/SUPPL_FILE/AO8B00769_SI_001.PDF

60. Xiang E, Moran CS, Ivanovski S, Abdal-hay A. Nanosurface Texturing for Enhancing the Antibacterial Effect of Biodegradable Metal Zinc: surface Modifications. *Nanomaterials*. 2023;13(13):2022. doi:10.3390/NANO13132022/S1

61. Preda VG, Săndulescu O. Communication is the key: biofilms, quorum sensing, formation and prevention. *Discoveries*. 2019;7(3):e10. doi:10.15190/d.2019.13

62. IX Y, Zhang J, IS Z, Mei ML, Li Q, Chu CH. The Antibacterial Mechanism of Silver Nanoparticles and Its Application in Dentistry. *Int J Nanomed*. 2020;15:2555–2562. doi:10.2147/IJN.S246764

63. Jang J, Choi Y, Tanaka M, Choi J. Development of silver/graphene oxide nanocomposites for antibacterial and antibiofilm applications. *J Ind Eng Chem*. 2020;83:46–52. doi:10.1016/J.JIEC.2019.11.011

64. Codiță I, Caplan DM, Drăgulescu EC, et al. Antimicrobial activity of copper and silver nanofilms on nosocomial bacterial species. *Roum Arch Microbiol Immunol*. 2010;69(4):204–212.